

Experimental Investigation of Droplets/Wall Interaction Relevant to Entrained-Flow Slagging Gasifiers

Maurizio Troiano^{a,*}, Fabio Montagnaro^b, Roberto Solimene^c, Piero Salatino^a

^a Dipartimento di Ingegneria Chimica, dei Materiali e della Produzione Industriale, Università degli Studi di Napoli Federico II, Piazzale Vincenzo Tecchio 80, 80125 Napoli (Italy).

^b Dipartimento di Scienze Chimiche, Università degli Studi di Napoli Federico II, Complesso Universitario di Monte Sant'Angelo, 80126 Napoli (Italy).

^c Istituto di Scienze e Tecnologie per l'Energia e la Mobilità Sostenibili, Consiglio Nazionale delle Ricerche, Piazzale Vincenzo Tecchio 80, 80125 Napoli, Italy
maurizio.troiano@unina.it

The phenomenology of droplets/wall interaction relevant to entrained-flow gasifiers has been investigated. The present study reports an experimental characterization of the sticking/spreading/rebound patterns during impact experiments of molten particles. A physical modelling approach was followed, by simulating the slag particles with synthetic wax particles impacted against a target at near-ambient conditions. The phases of impact, spread and deposition were characterized in terms of spread factor for different operating conditions. No rebound occurred under the tested conditions. Experimental data fairly well agreed with theoretical correlations from literature in terms of morphological evolution of the impacted droplets and excess rebound after collisions with the walls.

1. Introduction

The impingement of droplets on a solid surface occurs in both nature and industrial applications, such as sprays, coating, ink-jet printing. Liquid properties, surface wettability and roughness (Pan et al., 2009), wall temperature, impact velocity (Fujimoto et al., 2007) and impact angle are key factors determining the evolution of the morphology of the droplets upon the impact and the interaction patterns with a surface. Recently, some technologies have been considered to encourage energy saving and emission reduction, such as centrifugal granulation of molten blast furnace slag coupled with heat recovery and entrained-flow gasification. In these processes a crucial aspect is due to high-temperature and high-viscosity droplets impacting solid surfaces (He et al., 2019). As an example, in granulation process, the impingement of slag droplets with the wall is followed by spread, recoil, rebound phenomena while varying the impacting conditions (He et al., 2020). On the other hand, deposition and accumulation of slag on the walls reflect in lower heat recovery and slag quality (Yang et al., 2019). In entrained-flow slagging gasification reactors very high operating temperatures promote the onset of slagging of the ash residues. The generated slag sticks on the refractory walls, contributing to the formation of a slag layer. Above the softening point, ash becomes sticky and agglomerates causing plugging at the bottom exit or fouling of the heat exchange equipment (Troiano et al., 2017). Above the slagging temperature, ash has a fully liquid behaviour and it is easily drained from the bottom of the gasifier and eventually quenched as vitrified slag. Furthermore, the slag layer formation is able to trigger different regimes in the near-wall region of the gasifier, affecting fuel particles residence time and reactivity (Troiano et al., 2019). The efficiency of ash collection on a deposition probe sharply increased to a maximum as the carbon conversion approached a critical value, to slightly decrease thereafter (Li and Whitty, 2012). This result confirms that the effective ash stickiness depends on the residual carbon content in the particle (Troiano et al., 2020). To provide guidelines to the operation of this kind of processes, a full knowledge of slag impact behavior is required (Kleinhans et al., 2018). Ni et al. (2011) proposed a sub-model based on energy balances for predicting the slag droplets interaction with the wall, hence the slag layer formation. They specifically investigated the effects of slag viscosity, impact velocity, impact angle, molten slag surface tension and particle size on the maximum spread

diameter and on the rebound criterion, as developed by Pasandideh-Fard et al. (1996) and Mao et al. (1997). The prediction performance of the energy conservation-based model is dependent on the prediction of the maximum spread factor during the impaction process. However, the spread factor was derived from the spreading of water droplets with particle Reynolds number much higher than that for the slag. The current energy conservation-based particle sticking/rebounding model still needs further development.

The present study reports an experimental characterization of the sticking/spreading/rebound patterns during impact experiments of molten particles. A physical modelling approach was followed, by simulating the real process with synthetic wax particles impacted against a target at near-ambient conditions.

2. Experimental

A schematic of the experimental apparatus used in the present study for the collision behaviour of liquid droplets with a solid surface is shown in Figure 1. A detailed description of the experimental procedure is reported elsewhere (Troiano et al., 2014). The plastic/fluid behavior of softened or molten ash and of the wall slag layer has been simulated, at nearly ambient conditions, by molten wax as a surrogate of fuel ash. Waradur E™ (Völpker Spezialprodukte, Germany) was selected, as the rheological/mechanical properties of this wax (a refined material made from black raw montan wax) resembled those of a typical coal slag (Troiano et al., 2016). The wax was liquefied and stored in a heated vessel, before being conveyed to an atomization nozzle. The atomization zone consisted of a plenum chamber, including a distributor plate, an atomizer positioning section and the nozzle. The atomization system generated a spray of molten wax in the model reactor which eventually gave rise, upon deposition onto the wall, to a layer of molten wax. The nozzle was a commercial Delavan™ air-assisted atomizer (AL model), designed so as to generate a spray of conical shape with an aperture angle of $\theta_{\max} = 22\text{--}25^\circ$ and a uniform cross-sectional distribution of droplets of 10–100 μm size. The atomization air was preheated and fed directly to the nozzle, while a mainstream of air was preheated and fed sideways the atomization zone, flowing through a plenum chamber and a distributor plate in order to equalize the distribution of the mainstream air across the reactor. The reactor consisted of a Pyrex™ tube ($D = 0.10$ m-ID) on which the atomizing system was fitted. The flow rate of mainstream air, Q_{ms} , was treated as parameter for the purposes of evaluating the effect of different fluid dynamic conditions on the phenomenology of interaction between the lean-dispersed phase and the wall layer.

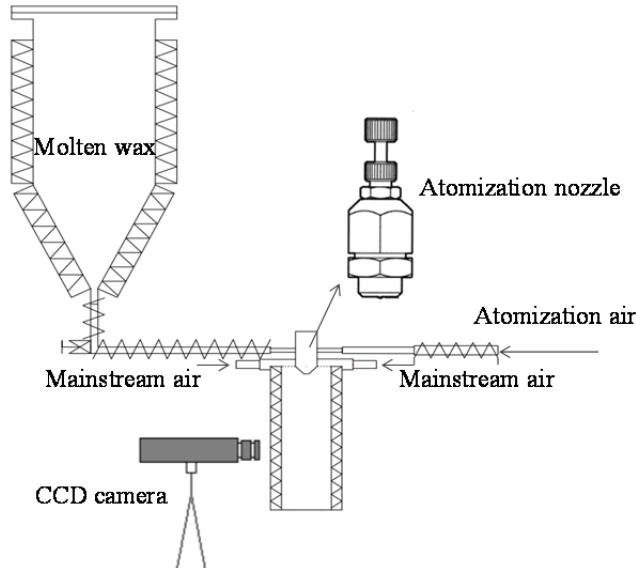


Figure 1: Scheme of the experimental apparatus.

Visual observation of droplet impingement on the wall was accomplished with a progressive scan CCD camera (Photron Ultima APX), equipped with a magnifying zoom lens and a 27.5 mm extension tube. The frame-by-frame recording was accomplished at a sampling rate of 2000 fps, with a 0.028 m \times 0.028 m recording window digitized as 1024 \times 1024 square pixels (spatial resolution equal to about 27 μm), while the shutter time was set to 42 μs .

Visual observation and video recording allowed to characterize the near-wall interactions, from a phenomenological and qualitative point of view. The video recordings were useful to evaluate the maximum

spread factor $\xi = D_{max}/D_0$. As the impact is oblique, the shape of the droplet at the maximum spread will be elliptical. As a matter of fact, it is possible to see the spherical droplet approaching the wall (Figure 2, first frame) and the elliptical shape at its maximum spread (Figure 2, fifth frame), where d_x and d_y are the minor and major ellipse axes, respectively. The elliptical splat area can be converted into an equivalent splat of circular shape and its equivalent diameter, $D_{max,eq}$, can be derived. It is possible to define the equivalent diameter $D_{max,eq} = \sqrt{d_x d_y}$ as the diameter of a circular splat with the same area as the elongated splat (Kang and Ng, 2006).

Analysis of video recordings enabled to track the fate of individual droplets. It was possible to see the phases of impact, spread and deposition, while no rebound occurred. Furthermore, the spreading phase was, in some events, accompanied by the phenomenon of fingering, which is the separation of a part of the liquid from the elliptical splat. The fingering is the result of an instability at the spreading edge of the splat, and it is typically unidirectional.

The CCD camera was located at 0.1 m from the nozzle and two mainstream gas flow rates ($Q_{ms}=1 \text{ m}^3 \text{ h}^{-1}$ and $Q_{ms}=10 \text{ m}^3 \text{ h}^{-1}$) were investigated, while the atomization air flow rate Q_a was fixed at $0.275 \text{ m}^3 \text{ h}^{-1}$.

3. Results and discussion

A typical impact event of a droplet with the spreading phase and an impact event for which fingering occurred are reported in Figure 2 and Figure 3, respectively.

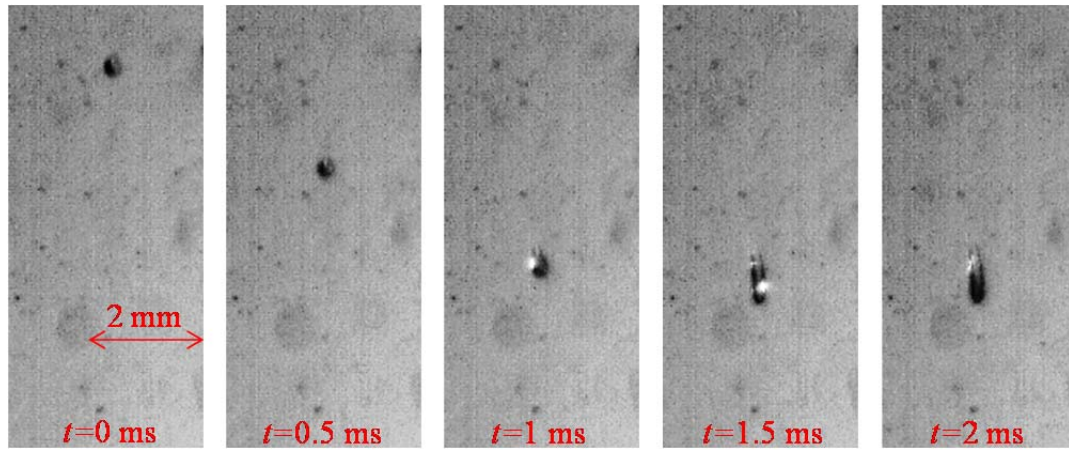


Figure 2: Impact of a wax droplet on the Pyrex duct wall with spreading and deposition phenomena.

Analysis of the frames allowed to determine the experimental spread factor, ξ for each tracked droplet. The spread factor was derived from energy balances for different impact stages: pre-impact (stage A), maximum spread (stage B), maximum recoil, sticking/rebound (Mao et al., 1997). It is possible to calculate the energy before and after each stage considering kinetic energy, surface energy and viscous dissipation energy and to model the maximum spread and the rebound phenomena. The kinetic energy (E_{KA}) and surface energy (E_{SA}) in stage A are:

$$E_{KA} = \frac{1}{2} m v_i^2 = \left(\frac{1}{2} \rho_D v_i^2 \right) \left(\frac{1}{6} \pi D_0^3 \right) \quad (1)$$

$$E_{SA} = A \gamma_{LV} = \pi D_0^2 \gamma_{LV} \quad (2)$$

At the impact stage (stage B), kinetic energy (E_{KB}) is zero, while the surface energy is:

$$E_{SB} = \left(\frac{\pi}{4} D_{max}^2 + \frac{2}{3} \pi \frac{D_0^3}{D_{max}} \right) \gamma_{LV} + \frac{\pi}{4} D_{max}^2 (\gamma_{SL} - \gamma_{SV}) = \left(\frac{\pi}{4} D_{max}^2 (1 - \cos \theta_c) + \frac{2}{3} \pi \frac{D_0^3}{D_{max}} \right) \gamma_{LV} \quad (3)$$

The energy dissipated during the impact can be expressed as:

$$E_{diss,A-B} = 0.2 \frac{We^{0.83}}{Re^{0.33}} \left(\frac{D_{max}}{D_0} \right)^2 \pi D_0^2 \gamma_{LV} \quad (4)$$

where m , ρ_D , v_i , D_0 and D_{max} are the mass, the density, the impact velocity, the initial diameter and the maximum diameter of the droplet, respectively; γ_{SL} , γ_{LV} and γ_{SV} are the solid-liquid, liquid-vapor and solid-

vapor surface tensions, respectively. θ_c is the contact angle between the droplet and the surface, We is the Weber number, Re is the Reynolds number.

The energy conservation equation between the stages (A) and (B) can be expressed as:

$$E_{KA} + E_{SA} = E_{KB} + E_{SB} + E_{diss,A-B} \quad (5)$$

Substituting Equations (1)-(4) into (5) yields an expression for the maximum spread factor:

$$\left[\frac{1}{4}(1 - \cos\theta_c) + 0.2 \frac{We^{0.83}}{Re^{0.33}} \right] \xi^3 - \left(\frac{We}{12} + 1 \right) \xi + \frac{2}{3} = 0 \quad (6)$$

It is also possible to formulate a rebound criterion on the basis of the spread factor ξ . Mao et al. (1998) proposed a rebound criterion defining an excess rebound energy, ERE, calculated as the energy in the recoil stage normalized to the energy in the rebound stage. The rebound criterion can be expressed as:

$$ERE = 0.25(\xi)^2(1 - \cos\theta_c) - 0.12(\xi)^{2.3}(1 - \cos\theta_c)^{0.63} + \frac{2}{3\xi} - 1 \quad (7)$$

ERE describes the tendency of a droplet to rebound upon the impact. The limit condition is represented by $ERE = 0$, for which the energy at maximum recoil is equal to that at rest; when $ERE > 0$ it means that the energy at the recoil stage is larger than that in the rebound stage, thus the droplet will rebound; when $ERE \leq 0$ the droplet will stick on the surface.

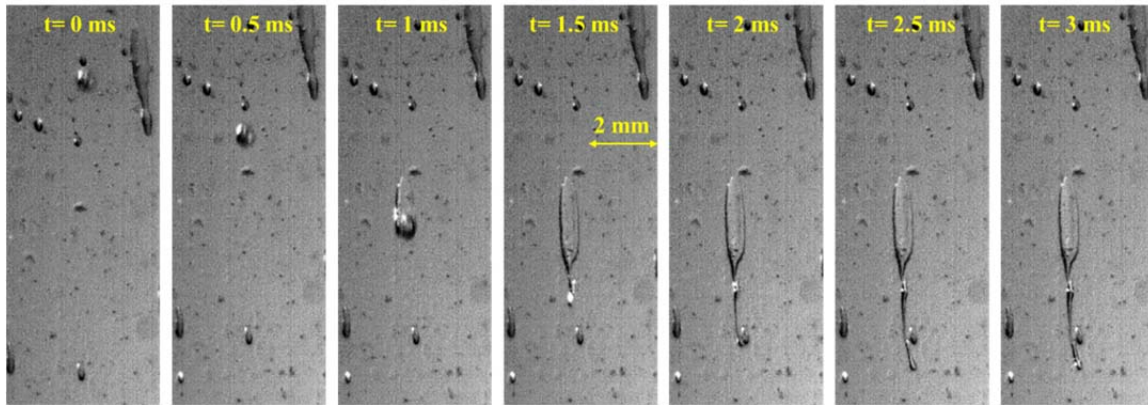


Figure 3: Impact of a wax droplet on the Pyrex duct wall with deposition after spreading and fingering phenomena.

Figure 4 reports the spread factor ξ as a function of the Weber number We . ξ does not significantly vary with the Weber number and it is $\xi=1.8\pm0.05$. This outcome indicates that deposition is the main interaction regime between droplets and wall. In Figure 4 the experimental data points of ξ are also compared with the theoretical model (Mao et al., 1997). In the theoretical calculation of ξ , the droplet viscosity is set equal to $\mu = 0.02$ Pa s, while the contact angle is $\theta_c=85\pm2^\circ$. Theoretical and experimental values agree fairly well for both the values of Q_{ms} . However, the experimental data points are about constant with the Weber number, whereas the theoretical values slightly increase with We . The difference may be due to the assumption, in the theoretical model, of a circular splat. As a matter of fact, the model was proposed for normal impacts. For oblique impacts, the splat can be better approximated by an ellipse. The equivalent elliptical-to-circular diameter was calculated to compare the experimental results with the theoretical model. Thus, the discrepancy between the experimental and theoretical values could be due to the procedure of spread factor calculation. Furthermore, the video recording system did not allow to measure the impact angle for each droplet, while a constant value was used, equal to the jet aperture angle. A difference in the impact angle could lead to different impact velocity components and, thus, to different spread factors.

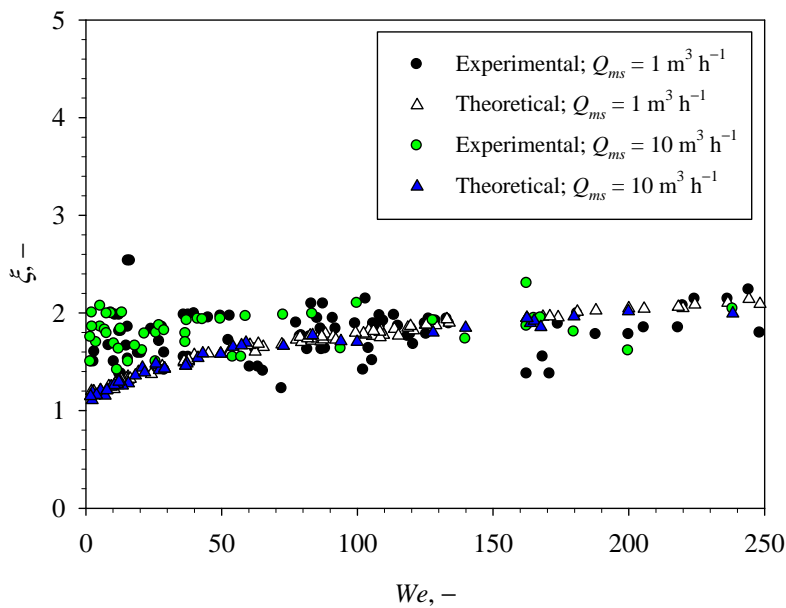


Figure 4: Effect of the mainstream air flow rate Q_{ms} on the spread factor, ξ , as a function of the Weber number, We .

Figure 5a) reports the trend of the excess rebound energy, ERE , as a function of the initial droplet diameter D_0 , for the two values of Q_{ms} ($1 \text{ m}^3 \text{ h}^{-1}$ and $10 \text{ m}^3 \text{ h}^{-1}$). For each case the experimental values of ERE are lower than 0 for D_0 ranging between $1.2 \cdot 10^{-4} \text{ m}$ and $4.8 \cdot 10^{-4} \text{ m}$. This outcome ($ERE < 0$) confirms that adhesion is the phenomenon which characterizes this kind of droplet-wall interaction. Ni et al. (2011) used the model proposed by Mao et al. (1997) to predict the slag-wall interaction in entrained-flow slagging gasifiers. Results obtained by the experimental tests with wax can be compared with those obtained by Ni et al. (2011), as reported in Figure 5b) for a fixed impact velocity equal to 4.5 m s^{-1} . Physical properties of wax and Shenfu coal slag are reported in Table 1.

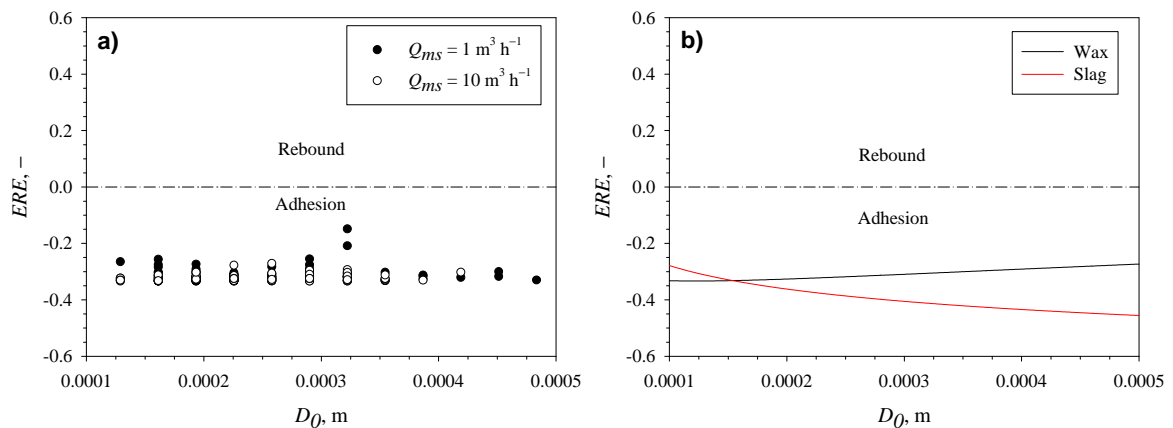


Figure 5: Effect of the droplet initial diameter on ERE . a) Experimental results obtained while varying the air flow rate; b) comparison between experimental results obtained with wax droplets and modelling results for slag droplets.

It is noteworthy in Figure 5b) that the excess rebound energy ERE is lower than 0 for both wax and slag droplets. From a quantitative point of view, the curves are different and the main reason lies in the different contact angle, i.e. the wettability, between the droplets and the wall. Finally, it is possible to conclude that wax mimics very well the build-up of the slag layer on the walls of the gasifier.

Table 1: Physical properties of montan wax and Shenfu coal slag.

	Waradur E wax	Shenfu coal slag
ρ ($kg\ m^{-3}$)	1000	2715
μ ($Pa\ s$)	0.02 (at 110°C)	0.65 (at 1500 °C)
γ ($N\ m^{-1}$)	0.029	0.4
θ_c (°)	85	56

4. Conclusions

In this study, the impact-deposition-rebound dynamical patterns of droplets colliding with duct walls have been investigated using high speed imaging. Experiments were carried out using montan wax to simulate and gain useful insight on the micromechanics of slag–wall interaction relevant to entrained-flow gasification. Under considered operating conditions in terms of impact velocity and impact angle, deposition is the prevailing droplet–wall interaction. Experimental results well agreed with a theoretical model in terms of evolution of the spread factor of the droplets upon the impact with the wall. Furthermore, a rebound criterion was successfully applied for the operating conditions under evaluation which can be useful to predict slag deposition in entrained-flow furnaces and gasifiers.

References

- Fujimoto H., Shiotani Y., Tong A.Y., Hama T., Takuda H., 2007, Three-dimensional numerical analysis of the deformation behavior of droplets impinging onto a solid substrate, *International Journal of Multiphase Flow*, 33, 317–332.
- He X.Y., Zhu X., Wang H., Tan Y., Ding B., Liao Q., 2019, Experimental visualization and theoretical analysis of the dynamic impact behavior of a molten blast furnace slag droplet on different surfaces, *Applied Thermal Engineering*, 147, 1–9.
- He X.Y., Zhu X., Wang H., Tan Y., Ding B., Lv Y.W., Liao Q., 2020, Dynamic behaviors and regime map of a molten blast furnace slag droplet impacting a solid surface, *Fuel*, 279, 118451.
- Kang C.W., Ng H.W., 2006, Splat morphology and spreading behavior due to oblique impact of droplets onto substrates in plasma spray coating process, *Surface and Coatings Technology*, 200, 5462–5477.
- Kleinhans U., Wieland C., Frandsen F.J., Spliethoff H., 2018, Ash formation and deposition in coal and biomass fired combustion systems: Progress and challenges in the field of ash particle sticking and rebound behavior, *Progress in Energy and Combustion Science*, 68, 65–168.
- Li S., Whitty K.J., 2012, Physical phenomena of char-slag transition in pulverized coal gasification, *Fuel Processing Technology*, 95, 127–136.
- Mao T., Kuhn D.C.S., Tran H., 1997, Spread and rebound of liquid droplets upon impact on flat surfaces, *AIChE Journal*, 43, 2169–2179.
- Ni J., Yu G., Guo Q., Zhou Z., Wang F., 2011, Submodel for predicting slag deposition formation in slagging gasification systems, *Energy Fuels*, 25, 1004–1009.
- Pan K.L., Chou P.C., Tseng Y.J., 2009, Binary droplet collision at high Weber number, *Physical Review E*, 80, 036301.
- Pasandideh-Fard M., Qiao Y.M., Chandra S., Mostaghimi J., 1996, Capillary effects during droplet impact on a solid surface, *Physics of Fluids*, 8, 650–659.
- Troiano M., Montagnaro F., Salatino P., Solimene R., 2017, Experimental characterization of particle-wall interaction relevant to entrained-flow gasification of biomass, *Fuel*, 209, 674–684.
- Troiano M., Montagnaro F., Solimene R., Salatino P., 2019, Modelling entrained-flow slagging gasification of solid fuels with near-wall particle segregation, *Chemical Engineering Journal*, 377, 119962.
- Troiano M., Salatino P., Solimene R., Montagnaro F., 2014, Wall effects in entrained particle-laden flows: The role of particle stickiness on solid segregation and build-up of wall deposits, *Powder Technology*, 266, 282–291.
- Troiano M., Solimene R., Salatino P., Montagnaro F., 2016, Multiphase flow patterns in entrained-flow slagging gasifiers: Physical modelling of particle–wall impact at near-ambient conditions, *Fuel Processing Technology*, 141, 106–116.
- Troiano M., Solimene R., Montagnaro F., Salatino P., 2020, Char/ash deposition and near-wall segregation in slagging entrained-flow gasification of solid fuels: from experiments to closure equations, *Fuel*, 264, 116864.
- Yang X., Ingham D., Ma L., Troiano M., Pourkashanian M., 2019, Prediction of particle sticking efficiency for fly ash deposition at high temperatures, *Proceedings of the Combustion Institute*, 37, 2995–3003.